

Ionization of the hydrogen atom in strong magnetic fields.

Beyond the adiabatic approximation

A.Y. Potekhin^{1,2,3}, G.G. Pavlov^{4,1}, and J. Ventura^{2,3}

¹ Ioffe Physical-Technical Institute, 194021, St.-Petersburg, Russia

² Department of Physics, University of Crete, 710 03 Heraklion, Crete, Greece

³ Institute of Electronic Structure and Laser, FORTH, 711 10 Heraklion, Crete, Greece

⁴ Pennsylvania State University, 525 Davey Laboratory, University Park, PA 16802, USA

Received 20 February 1996 / Accepted April 1996

Abstract. High magnetic fields in neutron stars, $B \sim 10^{11} - 10^{13}$ G, substantially modify the properties of atoms and their interaction with radiation. In particular, the photoionization cross section becomes anisotropic and polarization dependent, being strongly reduced when the radiation is polarized perpendicular to the field. In a number of previous works based on the adiabatic approximation the conclusion was drawn that this transverse cross section vanishes for frequencies ω smaller than the electron cyclotron frequency $\omega_c = eB/(m_e c)$. In other works (which employed a different form of the interaction operator) appreciable finite values were obtained, $\sim \sigma_0 \gamma^{-1}$ near the photoionization threshold, where σ_0 is the cross section without magnetic field, and $\gamma = B/(2.35 \times 10^9 \text{ G})$. Since it is the transverse cross section which determines the properties of radiation emitted from neutron star atmospheres, an adequate interpretation of the neutron star thermal-like radiation requires a resolution of this controversy.

In the present work we calculate the atomic wave functions for both discrete and continuum states by solving the coupled channel equations allowing the admixture between different Landau levels, which provides much higher accuracy than the adiabatic approximation. This enables us to resolve the above contradiction in favour of the finite transverse cross sections at $\omega < \omega_c$. Moreover, for any form of the interaction operator the non-adiabatic corrections appear to be substantial for frequencies $\omega \gtrsim 0.3\omega_c$. The non-adiabatic treatment of the continuum includes coupling between closed and open channels, which leads to the autoionization of quasi-bound energy levels associated with the electron cyclotron (Landau) excitations and gives rise to Beutler–Fano resonances of the photoionization cross section. We calculate the autoionization widths

of these quasi-bound levels and compare them with the radiative widths. The correlation of the open channels is responsible for the modification of the cross section above the Landau thresholds. The results are important for investigations of the radiation emergent from the surface layers of neutron stars.

Key words: atomic processes: photoionization – atomic processes: autoionization – magnetic fields – stars: neutron

1. Introduction

The proper interpretation of the recently discovered surface radiation of isolated pulsars (e.g., Ögelman 1995) requires knowledge of the elementary processes in magnetic neutron star atmospheres (Pavlov et al. 1995). Among such processes, ionization of atomic hydrogen is important both conceptually, due to the simplicity of the hydrogen atom, and practically, because of the presumably strong gravitational stratification of the neutron star atmospheres.

Although the photo- and autoionization of atoms have been thoroughly investigated at the magnetic field strengths $B \sim 10^5 - 10^9$ G (e.g., Merani et al. 1995, and references therein), none of these works can be directly extended to the typical pulsar field strengths $B \gtrsim 10^{11}$ G. First, the atomic wave functions at the pulsar fields are nearly cylindrical, while at $B = 10^9$ G the ground state atom is still nearly spherical. Second, the Landau levels at the pulsar fields are displaced much more distantly, which alters the spectrum qualitatively. These qualitative features arise when the parameter $\gamma = \hbar\omega_c/(2\text{Ry}) = B/(2.35 \times 10^9 \text{ G})$ exceeds unity. Here $\omega_c = eB/(m_e c)$ is

the electron cyclotron frequency, and $Ry = m_e e^4 / (2\hbar^2) = 13.6$ eV is the Rydberg energy.

The photoionization processes at $\gamma \gg 1$ have been considered in a number of papers: first analytically by Hasegawa & Howard (1961) and Gnedin et al. (1974), and then both analytically and numerically by Schmitt et al. (1981), Wunner et al. (1983b), Mega et al. (1984), Miller & Neuhauser (1991), Potekhin & Pavlov (1993) (hereafter Paper I), Bezchastnov & Potekhin (1994) (B&P), and Kopidakis et al. (1996) (KVH). All these papers, except for the two latter ones, employed the *adiabatic approximation* for the atomic wave functions. B&P and KVH studied the effect of atomic motion across the field on the photoionization process. Here we consider the particular case of atoms at rest. In this case the approach of KVH, who did not include electron cyclotron excitations, reduces back to the adiabatic one. There was no non-adiabatic treatment of the *final* state by B&P or by KVH.

The photoionization cross sections obtained in the cited papers appeared to be strikingly different. Some authors (e.g., KVH) concluded that, for the non-moving atom, the cross section for photons polarized perpendicular to the field vanishes in the most important frequency range $\omega < \omega_c$, while others (e.g., Paper I) presented finite transverse cross sections which, although suppressed by the strong magnetic field, are still significantly larger than, e.g., the Thomson cross section. Since the properties of radiation emitted from magnetic atmospheres are mainly determined by the transversely polarized photons (Pavlov et al. 1995), the different values of transverse cross sections should then result in quite different spectra and angular distributions of the radiation.

The first goal of the present paper is to resolve this contradiction, which is of crucial importance for modeling the neutron star atmospheres. We shall prove that the discrepancy is caused solely by using the adiabatic approximation and is eliminated as soon as this approximation is abandoned. The zero values of the transverse cross section arise from using the so-called velocity form of the interaction potential, which (contrary to the alternative length form) leads to inadequate results when used in the adiabatic approximation. The two representations yield the same nonzero transverse cross sections when the more accurate non-adiabatic approach is applied.

Our second principal goal is to extend the consideration of the photoionization to the domains of magnetic fields and photon energies where the adiabatic approximation does not provide sufficient accuracy. For instance, more than a dozen radio pulsars have magnetic fields in the range $\sim 10^{10} - 10^{11}$ G; the corresponding dimensionless fields, $\gamma \sim 4 - 40$, although they exceed unity, are not sufficiently high to neglect the non-adiabatic effects on the atomic properties. The non-adiabatic effects are also expected to be considerable for photon energies not very small as compared to the electron cyclotron energy, $\hbar\omega_c \simeq 1.2(B/10^{11} \text{ G})$ keV (Paper I). The spectral flux is

maximal at these X-ray energies for effective temperatures $\sim 4 \times 10^6 (B/10^{11} \text{ G})$ K characteristic of hot polar caps of radio pulsars. Such radiation has been observed from a number of pulsars by *ROSAT*, and new observations are under way with *ASCA*. For lower temperatures, more typical at the surfaces of cooling neutron stars, the radiation of such energies is still observable from nearby objects.

Among the non-adiabatic effects, particularly interesting are some new qualitative features of photoionization, which arise from including non-adiabatic terms in the final (continuum) state as well as in the initial state. In this approach, due to coupling to the continuum of lower Landau levels, the autoionization of quasi-bound atomic states, enters naturally into the consideration, giving rise to the so-called Beutler–Fano resonances below the thresholds of the electron cyclotron excitations. Comparison of the autoionization widths of the quasi-bound levels with the radiative widths shows that autoionization is important at relatively low fields, $B \lesssim 3 \times 10^{11}$ G. Our results demonstrate that the corresponding spectral features are expected to be observable in the thermal-like spectra of neutron stars with the next generation of X-ray satellites (particularly, *ASTRO-E*). In addition, above the electron cyclotron thresholds, different ionization channels are no longer independent of each other (as they were in the adiabatic approximation). The correlation of the channels is responsible for considerable modification of the photoionization cross sections, which should be observable in the spectra and light curves of the EUV/X-ray radiation of neutron stars.

2. Atomic wave functions

2.1. Coupled channel equations

The early studies of the hydrogen atom in strong magnetic fields have been based on the adiabatic approximation (e.g., Canuto & Ventura 1977). In this approximation the wave function of the relative motion $\psi_{s\eta}(\mathbf{r})$ is factorized into a transverse part $\Phi_{n,s}(\mathbf{r}_\perp)$ and a longitudinal part $g_n^{s\eta}(z)$, where z is the relative coordinate along the magnetic field, and $\mathbf{r}_\perp = (x, y)$. The transverse part is just the Landau function which describes the transverse motion of a free electron in a magnetic field, n being the Landau quantum number, and s the negative of the z -projection of the electron orbital momentum ($n \geq 0$, $s \geq -n$). The quantum number $\eta = \pm 1$ refers to the z -parity of the wave function. If the atom does not move as a whole across the field, which is the case of interest here, both η and s are exact quantum numbers, whereas n can be considered as a “good quantum number” at $\gamma \gg 1$. The longitudinal wave function $g_n^{s\eta}(z)$ obeys a one-dimensional Schrödinger equation with a potential obtained by averaging the Coulomb potential over the transverse coordinates.

The total energy of an atom is the sum of the longitudinal and transverse energies, $E = E^{\parallel} + E_{ns}^{\perp}$, with

$$E_{ns}^{\perp} = [n + (n + s)m_e/m_p] \hbar\omega_c, \quad (1)$$

where the term $(n+s)m_e/m_p$ accounts for the finite proton mass (Herold et al. 1981).

In more recent studies the atomic wave functions have been calculated using various numerical approaches (e.g., Xi et al. 1992, and references therein). At $\gamma \gtrsim 1$, the most convenient approach has been proposed by Simola & Virtamo (1978) and developed by Rösner et al. (1984) and Potekhin (1994) (Paper II). It is based on the expansion of the wave function over the complete orthogonal set of the Landau functions Φ_{ns} in the xy plane. Since, for non-moving atoms, s is an exact quantum number, the corresponding sum drops out, and we arrive at the reduced expansion

$$\psi_{s\eta}(\mathbf{r}) = \sum_{n'=n_{\min}}^{\infty} \Phi_{n's}(\mathbf{r}_{\perp}) g_{n'}^{s\eta}(z), \quad (2)$$

where $n_{\min} = 0$ for $s \geq 0$, and $n_{\min} = -s$ for $s < 0$. The functions $g_n^{s\eta}(z)$ can be found from the following system of coupled differential equations obtained by substituting the expansion (2) into the Schrödinger equation, multiplying it by $\Phi_{ns}^*(\mathbf{r}_{\perp})$ and integrating over \mathbf{r}_{\perp} ,

$$\begin{aligned} & \left[-\frac{\hbar^2}{2\mu} \frac{d^2}{dz^2} + V_{nn}^s(z) + E_{ns}^{\perp} - E \right] g_n^{s\eta}(z) \\ & = - \sum_{n' \neq n} V_{nn'}^s(z) g_{n'}^{s\eta}(z), \end{aligned} \quad (3)$$

where μ is the reduced mass. The set of the effective one-dimensional potentials is determined as

$$\begin{aligned} V_{nn'}^s(z) & = \langle ns | -e^2/r | n's \rangle_{\perp} \equiv (\Phi_{ns} | -e^2/r | \Phi_{n's}) = \\ & = -\frac{e^2}{a_m \sqrt{2}} \int_0^{\infty} I_{n+s,n}(\xi) I_{n'+s,n'}(\xi) (\xi + z^2/2a_m^2)^{-1/2} d\xi, \end{aligned} \quad (4)$$

where $I_{nn'}$ are the Laguerre functions (Sokolov & Ternov 1968), $a_m = a_B \gamma^{-1/2}$ is the magnetic length, and $a_B = \hbar^2/(m_e e^2)$ is the Bohr radius. Neglecting the non-diagonal ($n' \neq n$) effective potentials decouples the system and brings us back to the adiabatic approximation. The choice of the maximum Landau number n_{\max} for truncating expansion (2) is dictated by the desired accuracy — the more terms one retains the higher accuracy of the wave function is provided.

For any given set of the conserved quantities s and η , each term in expansion (2) is referred to as a *channel*, and the system (3) is the system of *coupled channel equations*. The whole set of $n_{\max} - n_{\min} + 1$ channels is separated into two groups. The first one includes *open channels* $n = n_{\min}, \dots, n_0 - 1$, for which $E > E_{ns}^{\perp}$. The second group embraces *closed channels* $n = n_0, \dots, n_{\max}$, for which the opposite inequality, $E < E_{ns}^{\perp}$, holds.

2.2. Bound states

In the adiabatic approximation, the right hand side in (3) vanishes and the channels are uncoupled. The bound states have negative longitudinal energies, i. e., correspond to the closed channels. The discrete energy levels are enumerated at specified s , and n by a longitudinal quantum number $\nu = 0, 1, 2, \dots$; the states having $\nu = 0$ are known as tightly bound, while those with $\nu \geq 1$ are hydrogen-like. The longitudinal quantum number fully determines the z -parity of the state, $\eta = (-1)^{\nu}$, so that the quantum number η becomes redundant and is usually omitted.

In the non-adiabatic approach, the RHS in (3) couples the state $|nsv\rangle$ into other channels, $n' \neq n$, comprising both bound states (closed channels) and continuum states (open). The wave functions $\psi_{nsv}(\mathbf{r}) = \sum_{n'} \Phi_{n's}(\mathbf{r}_{\perp}) g_{n'}^{nsv}(z)$ and the energy levels E_{nsv} can be designated by a *leading* term $n' = n$ of the expansion (2), if γ is large enough. Only the states with $n = n_{\min}$ can be truly bound. In other words, the energies E_{nsv} correspond to truly bound states only when all the channels are closed. Coupling of the closed channels shifts the level energies from the adiabatic values and admixes higher Landau orbitals to the bound state.

A non-adiabatic computer code for calculating the bound state wave functions of the hydrogen atom moving in a strong magnetic field has been described in Paper II. Here we apply this code (for the particular case of the non-moving atom) to obtain the initial state $|i\rangle$ of an atom subject to photoionization.

2.3. Continuum

The final atomic state $|f\rangle$ in the photoionization process lies in the continuum, $E_f > E_{n_{\min}s}^{\perp}$, i. e., at least one associated channel is open. All previous publications on photoionization in very strong magnetic fields treat the final state adiabatically, i.e. $\langle \mathbf{r} | f \rangle = \Phi_{ns}(\mathbf{r}_{\perp}) g^{(f)}(z)$. The simplest approach for the adiabatic continuum wave function is the Born approximation, used by Gnedin et al. (1974) for the non-moving atom and generalized by KVH to the case of motion across the field. It assumes the longitudinal wave function of the final state to be of the form

$$g^{(f)}(z) = \exp(\pm i k_n z), \quad (5)$$

where $k_n = \sqrt{2\mu(E_f - E_{ns}^{\perp})}/\hbar$ is the electron wave number, \pm denotes the direction of motion of the outgoing electron. A more accurate approach (e. g., Paper I) replaces $\exp(\pm i k_n z)$ by a function $g^{(f)}(z)$ numerically determined from the corresponding uncoupled equation; this function turns into (5) asymptotically, at $|z| \rightarrow \infty$ (up to a logarithmic phase factor).

In the non-adiabatic approach, the open (continuum) channel is coupled to closed channels and to other open channels (if the number of open channels $n_0 - n_{\min} > 1$).

This coupling of open and closed channels causes, in particular, autoionization of the quasi-bound states (states of positive energy which would be bound in the absence of coupling — see Section 2.4). The coupling of different open channels can be conveniently treated in terms of the *reactance matrix* $R_{nn'}$ (Seaton 1983). In the strong magnetic field case, the R -matrix can be introduced as follows.

System (3) of $n_{\max} - n_{\min} + 1$ coupled equations has (for a given parity η) $n_{\max} - n_{\min} + 1$ linearly independent solutions (basis vectors $g^{(n)s\eta} = [g_{n_{\min}}^{(n)s\eta}, \dots, g_{n_{\max}}^{(n)s\eta}]$) satisfying physically meaningful boundary conditions. It is convenient to enumerate the solutions similarly to the channels: $n = n_{\min}, n_{\min} + 1, \dots, n_{\max}$ (then $g_{n'}^{(n)s\eta} \rightarrow g_n^{(n)s\eta} \delta_{nn'}$ when the coupling switches off). Each of these solutions forms a wave function $\psi_{s\eta}^{(n)}(\mathbf{r}) = \sum_{n'} \Phi_{n's}(\mathbf{r}_{\perp}) g_{n'}^{(n)s\eta}(z)$ which comprises $n_0 - n_{\min}$ open channels and $n_{\max} - n_0 + 1$ closed channels. For unbound solutions ($n = n_{\min}, \dots, n_0 - 1$) of a given z -parity, it is sufficient to construct *real* longitudinal wave functions for positive z , which satisfy the following asymptotic conditions at $z \rightarrow +\infty$:

$$g_{n'}^{(n,\text{real})}(z) \sim \delta_{nn'} \sin \phi_{n'}(z) + R_{nn'} \cos \phi_{n'}(z) \quad (6)$$

for $n' = n_{\min}, \dots, n_0 - 1$, and $g_{n'}^{(n,\text{real})}(z) \rightarrow 0$ for $n' = n_0, \dots, n_{\max}$. (Hereafter, in this and the following subsections, we omit the indices s and η for brevity.) In Eq. (6),

$$\phi_{n'}(z) = k_{n'} z + (k_{n'} a_B m_e / \mu)^{-1} \ln(k_{n'} z) \quad (7)$$

is the z -dependent part of the phase. With the continuum wave functions normalized to unity in an interval of length L_z , the R -matrix satisfies the following symmetry relation,

$$k_{n'} R_{nn'} = k_n R_{n'n}. \quad (8)$$

The real basis of the wave functions $g_{n'}^{(n,\text{real})}(z)$ is convenient for calculations, but it still is to be transformed into the basis of outgoing waves, appropriate to photoionization. This is done by analogy with the usual theory (Seaton 1983). For an electron outgoing in the positive z direction, the following asymptotic condition at $z \rightarrow +\infty$ holds for the n -th solution:

$$g_{n'}^{(n,\text{out})}(z) \sim \delta_{nn'} \exp[i\phi_{n'}(z)] + S_{nn'}^{\dagger} \exp[-i\phi_{n'}(z)], \quad (9)$$

where S^{\dagger} is the Hermitean conjugate scattering matrix. Now, if we compose a $(n_0 - n_{\min}) \times (n_{\max} - n_{\min} + 1)$ matrix function $G(z)$ of the elements $g_{n'}^{(n)}(z)$ (with n the first and n' the second subscript), then we can obtain a set of the outgoing wave functions from the matrix equation

$$G^{(\text{out})} = 2i(1 + iR)^{-1} G^{(\text{real})}. \quad (10)$$

The S^{\dagger} matrix is expressed in terms of the R matrix as $S^{\dagger} = -(1 + iR)^{-1}(1 - iR)$.

Note that the longitudinal wave functions satisfying the asymptotic condition (9) should be multiplied by a common factor in order to ensure the correct normalization of the wave function $\psi^{(f,\text{out})}(\mathbf{r})$. It follows from the unitarity of the S -matrix that this factor equals $(2L_z)^{-1/2}$, where L_z is the z -extension of the periodicity volume of the final state.

2.4. Autoionizing states

The adiabatic and exact approaches treat in a fundamentally different way quasi-bound states associated with excited Landau levels. Since the adiabatic approximation allows no coupling between the Landau orbitals, a separate set of bound states appears below each Landau level n . These states, however, lie in the $n' < n$ continuum, and may therefore decay into the continuum via two processes. The first one is spontaneous emission of photons, which broadens these levels significantly in strong magnetic fields. This process has been thoroughly studied by Wunner et al. (1983a). The second one is *autoionization*, which could not be accounted for in the earlier work based on the adiabatic approach. In the non-adiabatic treatment, due to the coupling, the electron in a quasi-bound state can escape to infinity via any of the open channels $n' < n$.

The quasi-bound autoionizing states manifest themselves as resonances of the continuum wave function. For weaker magnetic fields ($\gamma < 1$) such states have been studied, e.g., by Friedrich & Chu (1983). Near a quasi-discrete level a resonance condition is satisfied, leading to a great amplification of the longitudinal coefficient $g_n(z)$. Thus, the shape of the wave function near the origin becomes similar to that calculated in the adiabatic approximation for the quasi-bound state. At large distances, where $g_n(z)$ decreases exponentially, the contribution of the orbitals $n' < n$ dominates, which can be interpreted as electron leakage from the quasi-bound state.

The general theory of autoionizing states has been described, e. g., by Friedrich (1991). Here we briefly discuss it for the case of the strongly magnetized hydrogen atom. Let the electron energy E be close to an energy $E_{n\nu}^{\text{ad}}$ at which there would be a bound state in the closed channel n in the absence of channel coupling. To consider coupling of the channel n to an open channel $n' < n$, one can retain the two corresponding terms in expansion (2) and two equations in the system (3), assuming there are no other quasi-discrete levels close to $E_{n\nu}^{\text{ad}}$. Let $g_{n'}^{\text{ad}}(z)$ and $\bar{g}_{n'}^{\text{ad}}(z)$ be the two linearly independent solutions for the uncoupled open channel (e. g., with asymptotic behaviour $g_{n'}^{\text{ad}}(z) \sim \sin[\phi_{n'}(z) + \delta_{\text{ad}}]$ and $\bar{g}_{n'}^{\text{ad}}(z) \sim \cos[\phi_{n'}(z) + \delta_{\text{ad}}]$ at $z \rightarrow \infty$, where δ_{ad} is the adiabatic phase shift, and $\phi_{n'}(z)$ is defined by Eq. (7)), and $g_{n\nu}^{\text{ad}}(z)$ be the solution for the uncoupled closed channel. Then, by analogy with the non-

magnetic case, the solution of the two coupled channel equations can be presented in the form

$$g_{n'}(z) = \cos \delta_c g_{n'}^{\text{ad}}(z) + \sin \delta_c \bar{g}_{n'}^{\text{ad}}(z), \quad (11)$$

$$g_{n\nu}(z) = -\sin \delta_c \frac{U_{n\nu, n'}}{\Gamma_{n\nu, n'}^{\text{a}}/2} g_{n\nu}^{\text{ad}}(z), \quad (12)$$

where δ_c is an additional asymptotic phase shift due to channel coupling,

$$\tan \delta_c = -\frac{\Gamma_{n\nu, n'}^{\text{a}}/2}{E - E_{n\nu}}. \quad (13)$$

In Eqs. (12) and (13),

$$\Gamma_{n\nu, n'}^{\text{a}} = \frac{2\mu L_z}{\hbar^2 k_{n'}} |U_{n\nu, n'}|^2 \quad (14)$$

is the (partial) *autoionization width* of the quasi-bound state $|n\nu\rangle$,

$$U_{n\nu, n'} = \int g_{n\nu}^{\text{ad}}(z) V_{n, n'}(z) g_{n'}^{\text{ad}}(z) dz \quad (15)$$

is the coupling matrix element, and $E_{n\nu}$ is the resonance energy (slightly shifted from $E_{n\nu}^{\text{ad}}$ — see Friedrich 1991). Note that Eqs. (14) and (15) can be derived directly with the help of the usual perturbation theory.

Thus, it follows from Eqs. (11) and (12) that coupling of the closed and open channels distorts the open channel wave function and admixes the bound state $|n\nu\rangle$ to the continuum. The strength of the admixture is given by the square of the amplitude in front of the bound wave function $g_{n\nu}^{\text{ad}}(z)$ in Eq. (12); its dependence on energy is determined by the resonance function (Breit–Wigner profile) which coincides with the derivative of the phase shift δ_c with respect to energy,

$$\frac{d\delta_c}{dE} = \frac{\Gamma_{n\nu, n'}^{\text{a}}/2}{(E - E_{n\nu})^2 + (\Gamma_{n\nu, n'}^{\text{a}}/2)^2}. \quad (16)$$

The closed channel n is most strongly coupled with the open channel $n' = n - 1$. If we want to include coupling with all the open channels, the total autoionization width can be evaluated as $\Gamma_{n\nu}^{\text{a}} = \sum_{n'=n_{\text{min}}}^{n-1} \Gamma_{n\nu, n'}^{\text{a}}$. As we shall see, the interference of the coupled states leads to the Beutler–Fano resonances in the energy dependence of the radiative transitions.

3. Interaction with radiation

3.1. Matrix element of the interaction

The cross section for ionizing an atomic state $|i\rangle$ into a continuum state $|f\rangle$ due to interaction with a photon of

frequency ω , wave vector \mathbf{q} , and polarization vector \mathbf{e} , can be written as (e.g., KVH)

$$\sigma_{i \rightarrow f} = \frac{3}{8\alpha^3} \frac{\text{Ry}}{\hbar\omega} \sqrt{\frac{\text{Ry}}{E_f}} \frac{L_z}{a_B} |\langle f | \hat{M} | i \rangle|^2 \sigma_{\text{Th}}, \quad (17)$$

where $\alpha = e^2/(\hbar c)$, and \hat{M} is the dimensionless interaction operator. Its “velocity” representation involves the kinetic momentum operator $\boldsymbol{\pi} = \mathbf{p} + (e/2c)\mathbf{B} \times \mathbf{r}$:

$$\hat{M}^{(\pi)} = \hat{M}_0^{(\pi)} + \delta\hat{M}^{(\pi)}, \quad (18)$$

where

$$\hat{M}_0^{(\pi)} = a_B \exp(i\mathbf{q}\mathbf{r}) \left[\frac{2}{\hbar} \mathbf{e} \cdot \boldsymbol{\pi} - i(\mathbf{q} \times \mathbf{e})_z \right], \quad (19)$$

and $\delta\hat{M}^{(\pi)}$ denotes corrections of order (m_e/m_p) . It will be shown that these corrections can be appreciable, when the velocity representation is used. Approximately one can write

$$\delta\hat{M}^{(\pi)} \approx \frac{m_e}{m_p} a_B \frac{2}{\hbar} \mathbf{e} \cdot \left(\mathbf{p} - \frac{e}{2c} \mathbf{B} \times \mathbf{r} \right). \quad (20)$$

The first term in the square brackets in Eq. (19) represents the electron current or “velocity” term in the interaction potential, while the second term corresponds to the interaction of the radiation magnetic field with the magnetic spin moment of the electron. We have neglected spin flip transitions, which are unimportant at $B \lesssim 10^{13}$ G, according to Wunner et al. (1983b) and KVH, and fixed the electron spin antiparallel to the magnetic field. Besides, we have omitted the term $\mathbf{e}\mathbf{q}$ (B&P) from the square brackets, assuming the transverse polarization.

Using Eq. (2) for both atomic states, we obtain

$$\langle f | \hat{M} | i \rangle = \sum_{nn'} \langle n, f | \langle n, s_f | \hat{M} | n', s_i \rangle_{\perp} | n', i \rangle_{\parallel}, \quad (21)$$

where the subscripts \perp and \parallel denote the transverse (cf. Eq. (4)) and longitudinal matrix elements, respectively. The inner (transverse) matrix element in Eq. (21) can be calculated analytically, using the well known properties of the electron Landau quantum states (e.g., Canuto & Ventura 1977), so that $\langle f | \hat{M} | i \rangle$ reduces to the sum of one-dimensional quadratures.

3.2. Transverse polarization: analytical consideration

Using the commutation relations for the Hamiltonian, the matrix element $\langle f | \hat{M} | i \rangle$ can be rewritten in the “length form” (Paper I):

$$\langle f | \hat{M}^{(\pi)} | i \rangle = \langle f | \hat{M}^{(r)} | i \rangle, \quad (22)$$

$$\hat{M}^{(r)} = \hat{M}_0^{(r)} + \delta\hat{M}^{(r)}, \quad (23)$$

$$\hat{M}_0^{(r)} = ia_B \exp(i\mathbf{q}\mathbf{r}) \left[\frac{2m_e\omega}{\hbar} \mathbf{e} \cdot \mathbf{r} \left(1 - \frac{\hbar\omega}{2m_e c^2} - \frac{\mathbf{q} \cdot \boldsymbol{\pi}}{m_e\omega} \right) - (\mathbf{q} \times \mathbf{e})_z \right]. \quad (24)$$

Here, as well as in Eq.(18), $\delta\hat{M}$ denotes corrections $\sim m_e/m_p$.

For exact atomic states $|i\rangle$ and $|f\rangle$, the two representations are equivalent. However, the equivalence (22) breaks down in the adiabatic approximation. The most striking difference occurs for transitions within the ground Landau state when the photons are polarized perpendicular to the magnetic field. It was recently confirmed by KVH that in this case $\langle 0, s_f | \hat{M}^{(\pi)} | 0, s_i \rangle_{\perp} = 0$ identically, if one neglects the small corrections due to $\delta\hat{M}^{(\pi)}$. One actually finds an exact cancellation of the contributions arising from the velocity and the spin interaction terms in Eq. (19). At the same time, the representation (24) leads to a non-zero cross section¹. Some analytical estimates help to resolve this apparent contradiction (see also Appendix A of Paper I).

Since series (21) converges rapidly at $\gamma \gg 1$, we can expect that it is sufficient to keep only the leading terms in it. In the velocity representation, the zero-order term $\langle 0, s_f | \hat{M}_0^{(\pi)} | 0, s_i \rangle_{\perp}$ vanishes (KVH). Retaining the first-order terms, we obtain

$$\begin{aligned} \langle f | \hat{M}^{(\pi)} | i \rangle &\approx \langle 1, f | \langle 1, s_f | \hat{M}_0^{(\pi)} | 0, s_i \rangle_{\perp} | 0, i \rangle_{\parallel} \\ &+ \langle 0, f | \langle 0, s_f | \hat{M}_0^{(\pi)} | 1, s_i \rangle_{\perp} | 1, i \rangle_{\parallel} \\ &+ \langle 0, f | \langle 0, s_f | \delta\hat{M}^{(\pi)} | 0, s_i \rangle_{\perp} | 0, i \rangle_{\parallel}. \end{aligned} \quad (25)$$

Which of the three terms in Eq. (25) dominates, depends on the magnetic field strength and transition considered.

In the length representation, the zero-order term dominates:

$$\langle f | \hat{M}^{(r)} | i \rangle \approx \langle 0, f | \langle 0, s_f | \hat{M}_0^{(r)} | 0, s_i \rangle_{\perp} | 0, i \rangle_{\parallel}. \quad (26)$$

Let us consider, for simplicity, the dipole approximation, $q \rightarrow 0$. It has been shown in Paper I (see also Sect. 4) that this approximation can be safely used at $\hbar\omega \ll \alpha m_e c^2 \ln \gamma \sim 300 \ln \gamma$ Ry. For $\theta = 0$, Eq. (25) then yields

$$\begin{aligned} \langle f | \hat{M}^{(\pi)} | i \rangle &\approx 2i \sqrt{\gamma} \left[e_+ (\langle 0, f | 1, i \rangle_{\parallel} + \zeta \sqrt{s_f}) \delta_{s_f, s_i+1} \right. \\ &\left. - e_- (\langle 1, f | 0, i \rangle_{\parallel} + \zeta \sqrt{s_i}) \delta_{s_f, s_i-1} \right], \end{aligned} \quad (27)$$

where $e_{\pm} = (e_x \pm i e_y) / \sqrt{2}$ are the cyclic components of the vector \mathbf{e} , and

$$\zeta = \frac{m_e}{m_p} \langle 0, f | 0, i \rangle_{\parallel}. \quad (28)$$

The terms with ζ represent the leading contribution due to $\delta\hat{M}^{(\pi)}$. Analogously, from Eq. (26) we obtain

$$\langle f | \hat{M}^{(r)} | i \rangle \approx 2i \sqrt{\gamma} \frac{\omega}{\omega_c} \left[e_+ \sqrt{s_f} \delta_{s_f, s_i+1} \right.$$

¹ The spin term $(q \times e)_z$, omitted in Paper I, cannot be responsible for this result, as was assumed by KVH. Indeed, the transverse cross section in Paper I remains non-zero even for photons directed along the field, in which case the spin term turns out to vanish identically.

$$\left. + e_- \sqrt{s_i} \delta_{s_f, s_i-1} \right] \langle 0, f | 0, i \rangle_{\parallel}. \quad (29)$$

Conditions under which Eqs. (27) and (29) give similar cross sections are obtained by equating their right-hand sides:

$$\langle 0, f | 1, i \rangle_{\parallel} \approx \sqrt{s_f} \left(\frac{\omega}{\omega_c} - \frac{m_e}{m_p} \right) \langle 0, f | 0, i \rangle_{\parallel}, \quad (30)$$

or

$$\langle 1, f | 0, i \rangle_{\parallel} \approx -\sqrt{s_i} \left(\frac{\omega}{\omega_c} + \frac{m_e}{m_p} \right) \langle 0, f | 0, i \rangle_{\parallel}, \quad (31)$$

where $s_f = s_i + 1$ or $s_i = s_f + 1$, respectively. The term m_e/m_p comes from $\delta\hat{M}^{(\pi)}$ through Eqs. (27), (28). Note that the terms m_e/m_p can give a substantial correction (especially near the photoionization thresholds, $\hbar\omega \sim \ln^2 \gamma$ Ry) in very strong fields, when $\gamma \ln^{-2} \gamma$ is not negligible in comparison with m_p/m_e .

Our analytical estimates (Appendix A) and numerical results (Sect. 4) confirm that the approximate relationships (30), (31) are indeed satisfied if $\omega \ll \omega_c$. Thus, in the adiabatic approximation (for $n = n' = 0$), the length representation of the interaction matrix element, employed in Paper I, enables one to calculate the leading contribution to the transverse cross section which is missed when the velocity representation is used. On the other hand, it makes no difference which representation is used if the post-adiabatic corrections are included.

3.3. Interference of open and closed channels: Beutler–Fano resonances

As we have discussed in Sect. 2.4, coupling of a closed channel n to open channels, particularly to the channel $n-1$, results in a resonance admixture of the quasi-bound state to the continuum. Interference of the two final coupled states leads to *Beutler–Fano resonances* in the photoabsorption spectrum (e. g., Friedrich 1991). According to Eqs. (11) and (12) (for $n' = n-1$), the transition matrix element, for the final electron energy close to the energy of the quasi-bound state, can be presented as

$$\langle f | \hat{M} | i \rangle = M_1 \cos \delta_c (1 - q \tan \delta_c), \quad (32)$$

where

$$q = \frac{M_2}{M_1} \frac{U_f}{\Gamma_f^a/2} \quad (33)$$

is the shape parameter of the Beutler–Fano resonance ($U_f \equiv U_{ns_f\nu_f, n-1}$, $\Gamma_f^a \equiv \Gamma_{ns_f\nu_f, n-1}^a$ — see Eqs. (14) and (15)),

$$M_1 = (g_{n-1, s_f}^{\text{ad}} | \langle n-1, s_f | \hat{M} | n_i s_i \rangle_{\perp} | g_{n_i s_i \nu_i} \rangle_{\parallel}) \quad (34)$$

is the matrix element in the absence of coupling,

$$\begin{aligned} M_2 = & -(\Gamma_f^a/2U_f) (\bar{g}_{n-1, s_f}^{\text{ad}} | \langle n-1, s_f | \hat{M} | n_i s_i \rangle_{\perp} | g_{n_i s_i \nu_i} \rangle_{\parallel}) \\ & + (g_{ns_f\nu_f}^{\text{ad}} | \langle ns_f | \hat{M} | n_i s_i \rangle_{\perp} | g_{n_i s_i \nu_i} \rangle_{\parallel}) \end{aligned} \quad (35)$$

is the coupling correction. The cross section is proportional to

$$\begin{aligned} |\langle f | \hat{M} | i \rangle|^2 &= |M_1|^2 \cos^2 \delta_c |1 - q \tan \delta_c|^2 \\ &= |M_1|^2 F(\epsilon, q), \end{aligned} \quad (36)$$

where

$$F(\epsilon, q) = \frac{|q + \epsilon|^2}{1 + \epsilon^2} \quad (37)$$

is the Beutler–Fano function,

$$\epsilon = -\cot \delta_c = 2(E - E_{n_s f \nu_f}) / \Gamma_f^a \quad (38)$$

is the reduced energy. The function $F(\epsilon, q)$ tends to unity in the very far wings of the resonance, at $|\epsilon| \gg \max(1, |q|)$. If q is real (e. g., in the dipole approximation), it turns to zero at $\epsilon = -q$ and is maximal ($F_{\max} = 1 + q^2$) at $\epsilon = 1/q$. In the limit of very weak coupling, $U_f \rightarrow 0$, we have $q \propto U_f^{-1} \rightarrow \infty$, $q^2 \Gamma_f^a$ remains finite, and the Beutler–Fano resonance turns into the delta-function (superimposed onto the bound-free continuum) which describes the bound-bound transition in the absence of coupling.

4. Results

We present here example photoionization cross sections, calculated in accordance with the approach described above. In all cases the hydrogen atom is assumed to be initially in its ground state. Basically we have employed the velocity representation of the interaction matrix element, including into $\hat{M}^{(\pi)}$ all the non-dipole and finite-mass corrections (Paper I), as well as the spin term (KVH). The results are compared with those obtained with the length representation, the adiabatic, and dipole approximations. Some details of the numerical techniques used are given in Appendix B.

Our first principal result is that at $\omega \ll \omega_c$ Eqs. (30) and (31) do hold with a high accuracy (the difference does not exceed 1–2% at $\hbar\omega \lesssim 30$ Ry), thus confirming the considerations of Sect. 3.2 and Paper I. In the calculations we have also included higher terms of the expansions (2) and (21); however, the channels $n, n' > n_f + 1$ proved to be unimportant. We have also checked the importance of the spin term, and found it to be negligible, by switching it on and off numerically. On the contrary, the corrections due to the finite proton mass are appreciable. If the terms m_e/m_p on the right-hand side of Eqs. (30), (31) were omitted, then the inaccuracy would increase to 10% at $\gamma = 1000$. Clearly, this would introduce an inaccuracy of about 20% in the cross section.

Figure 1 shows the cross section as a function of the photon energy $\hbar\omega$ for photoionization from the ground level, at a magnetic field strength $B = 10^{13}$ G ($\hbar\omega_c = 8509$ Ry); the cross sections plotted are for photons propagating along the magnetic field ($\theta = 0^\circ$) with the right circular polarization (σ_+), and propagating perpendicular

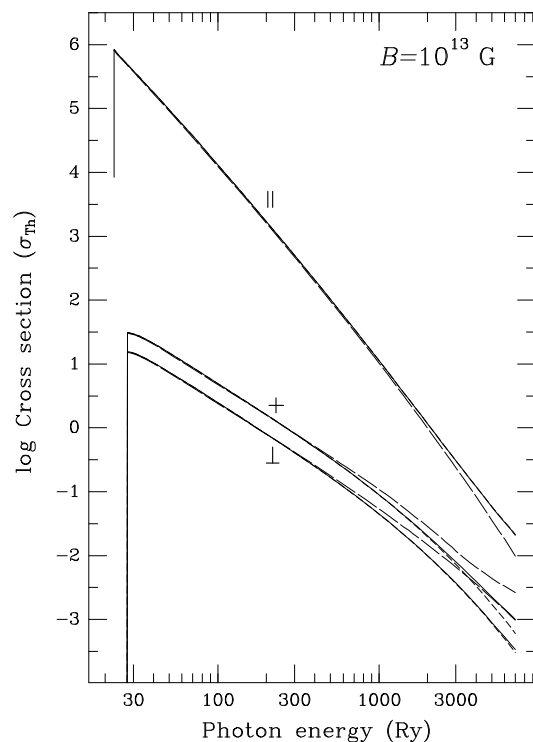


Fig. 1. Total cross sections of the photoionization of the ground state H atom at the magnetic field strength $B = 10^{13}$ G. The curves are labelled by the symbols $+$, \perp , and \parallel , corresponding respectively to σ_+ (right circular polarization at $\theta = 0^\circ$), σ_\perp (polarization vector transverse to B at $\theta = 90^\circ$), and σ_\parallel (polarization along B at $\theta = 90^\circ$). Numerical results (solid lines) are compared with the dipole approximation (short-dashed lines) and with the adiabatic results of Paper I (long-dashed lines)

to the field ($\theta = 90^\circ$) with the linear polarizations parallel (σ_\parallel) and perpendicular (σ_\perp) to \mathbf{B} . Short-dashed lines correspond to the dipole approximation. We see that at $\theta = 90^\circ$ the non-dipole corrections are unimportant for σ_\parallel and σ_\perp at $\hbar\omega \lesssim 10^4$ Ry. This confirms the validity of the transverse dipole approximation in this energy range and justifies neglecting the spin term, as it depends on the transverse wave vector only. On the other hand, the inaccuracy of the longitudinal dipole approximation becomes perceptible at $\hbar\omega \gtrsim (2 - 3) \times 10^3$ Ry, which is seen from the deviation of the short-dashed line from the solid one for σ_+ .

For comparison, the results of Paper I (length representation) which do not include the non-adiabatic and spin terms are shown by long-dashed lines. The agreement with the adiabatic approach of Paper I, which involved the length form of the interaction matrix element, is fairly good at $\hbar\omega \lesssim 10^3$ Ry. Note that the velocity form would lead to vanishing σ_+ and σ_\perp (KVH).

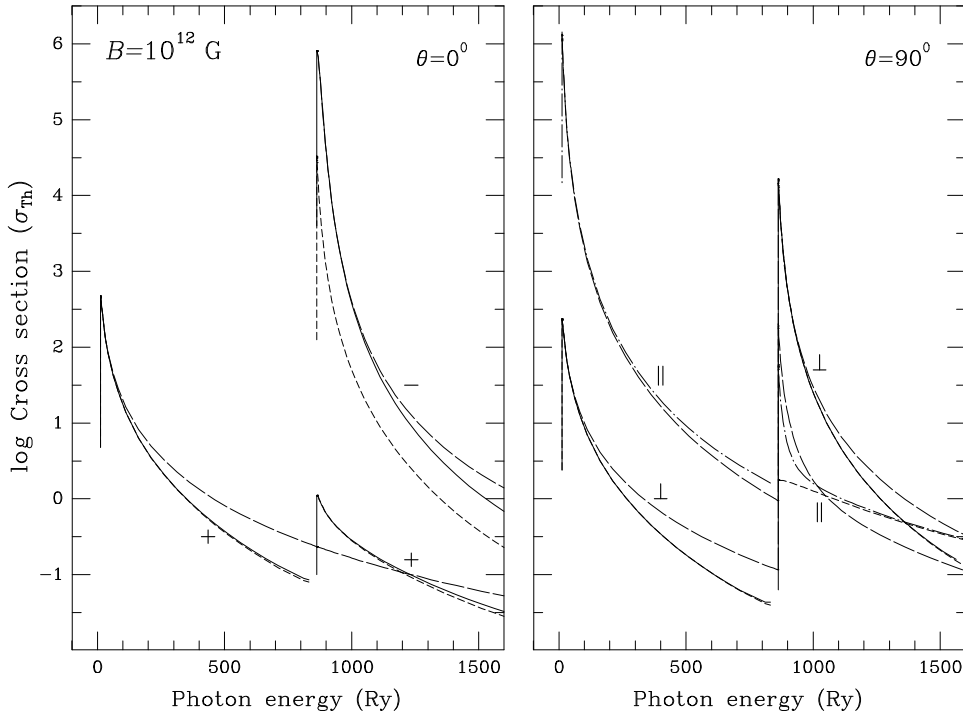


Fig. 2. Same as Fig. 1 for $B = 10^{12}$ G. The symbol ‘-’ corresponds to the left circular polarization at $\theta = 0^\circ$. Numerical results for σ_- and σ_\parallel are plotted with the dot-dashed line, numerical results for σ_+ and σ_\perp with the solid line. The long-dashed and short-dashed lines correspond to the adiabatic (Paper I) and dipole approximations, respectively. **a** Circular polarization (σ_\pm) at $\theta = 0^\circ$. **b** Linear polarization ($\sigma_\perp, \sigma_\parallel$) at $\theta = 90^\circ$

The agreement with the adiabatic results becomes worse as ω approaches ω_c from below, which is caused by the growing role of the “side” terms (closed channels $n > 0$) in Eq. (21). Figure 2 demonstrates the cross sections at $B = 10^{12}$ G ($\hbar\omega_c = 850.87$ Ry). We see that the adiabatic approximation (long dash) may serve only as an order-of-magnitude estimate at $\omega \sim \omega_c$, whereas at $\omega \lesssim (0.2 - 0.3)\omega_c$ the agreement is good again. For the magnetic field chosen, the channel $n = 1$ opens at the (threshold) energies $\hbar\omega = 862.79, 863.25$ and 863.72 Ry for $s_f = -1, 0$ and 1 , respectively (these would be the $n = 1$ thresholds for the left, right and longitudinal polarizations in the dipole approximation). Immediately above the thresholds, the adiabatic approximation for σ_- and σ_\perp becomes sufficiently accurate again, as has been predicted in Paper I. Photoionization from the ground state is strictly forbidden for the left polarization below the $n = 1$ threshold. Above the threshold, the corresponding cross section σ_- appears to be strongly underestimated in the dipole approximation (see the left panel of Fig. 2). The importance of the factor $\exp(iqr)$ in this case is explained by approximate coincidence of the photon and electron wave numbers, as discussed in Paper I. The dipole approximation is inadequate also for σ_\parallel (right panel of Fig. 2) above the $n = 1$ threshold because it misses the channel

$n = 1, s_f = -1$, which gives the main contribution just at these energies. For this polarization, the adiabatic approximation (long-dashed lines) proves to be inaccurate as well, mainly because of the admixture of the (open) channels $n = 0$ and $n = 1$.

The solid and short-dashed curves for the non-adiabatic cross sections presented in Fig. 2 do not include values within ~ 30 Ry just below the $n = 1$ threshold. Within this gap complex resonance structures arise in the photoionization cross sections, too narrow to be resolved in the scale of Fig. 2. An example of such structures is shown in an expanded scale in Fig. 3. The resonances are associated with the quasi-bound autoionizing states $|1, s_f, \nu_f\rangle$ admixed to the continuum $|0, s_f\rangle$. Their shape in the dipole approximation (short-dashed lines) is typical for the Beutler–Fano resonances (see Sect. 3.3) with a negative q parameter: the peaks (at $E = E_{1s_f\nu_f} + (2q)^{-1}\Gamma_{1s_f\nu_f}^a$) are followed by troughs (at $E = E_{1s_f\nu_f} - q\Gamma_{1s_f\nu_f}^a/2$). If $|q| \gg 1$ for a given resonance (which is fulfilled for the resonances shown in Fig. 3), then the FWHM of the peak coincides with the autoionization width $\Gamma_{1s_f\nu_f}^a$ (see Sect. 2.4), and the distance between the peak maximum and the trough minimum is $\simeq |q|\Gamma_{1s_f\nu_f}^a/2 \gg \Gamma_{1s_f\nu_f}^a$. For instance, for the main peak of $\sigma_+(E)$, which is associated with

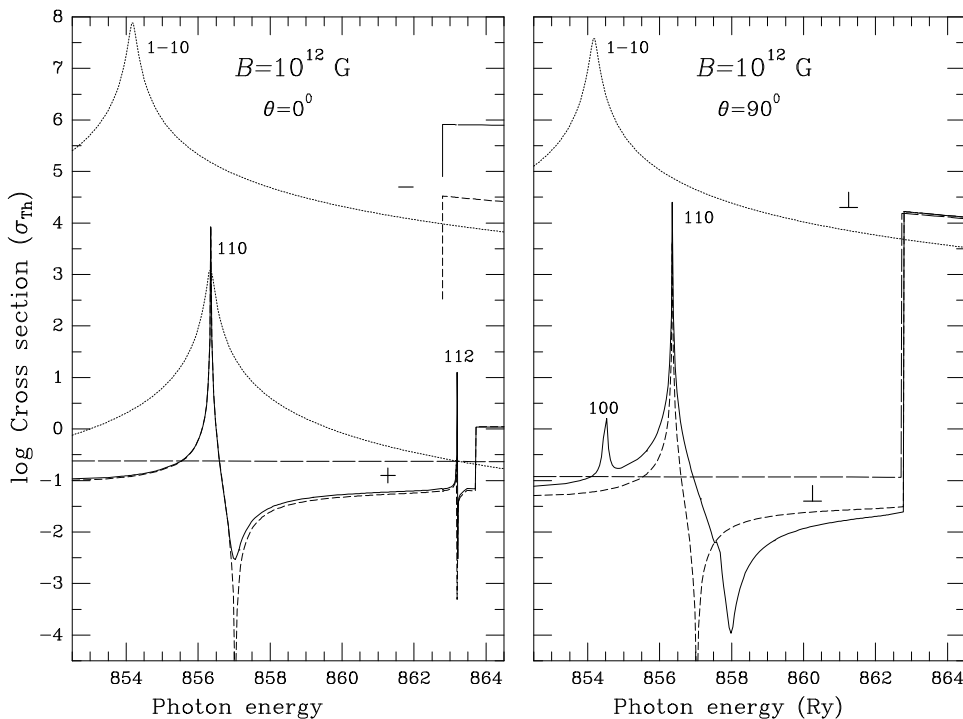


Fig. 3. Same as Fig. 2 in the energy range near the Landau threshold. **a** Circular polarization (σ_{\pm}) at $\theta = 0^{\circ}$. **b** Linear transverse polarization (σ_{\perp}) at $\theta = 90^{\circ}$. Superimposed on the same diagram, the dotted curves show the “bound-bound” absorption profiles calculated without allowance for coupling of the closed and open channels; the shapes of these profiles are determined by the radiative deexcitation of the upper levels (see text for details)

the autoionizing state $|1, 1, 0\rangle$, we have $\Gamma_{110}^a \simeq 0.01$ Ry and $q \simeq -200$. Resonances of the same nature have been obtained previously for the case of lower magnetic fields, $\gamma \ll 1$ (cf. Delande et al. 1991; O’Mahoni & Mota-Furtado 1991). For strong magnetic fields (and, consequently, higher photon energies), non-dipole corrections change the shape of the resonances so that the shape becomes different for different polarizations and angles θ . In particular, the parameter q is no longer real, which results in non-zero values of the trough minima shifted from their positions obtained in the dipole approximation. An additional effect entering when we go beyond the dipole approximation is the appearance of additional dipole-forbidden peaks overlapping with the dipole-allowed resonances. For instance, for σ_{\perp} , the peak at $\hbar\omega \simeq 856.4$ Ry, associated with the quasi-bound state $|1, 1, 0\rangle$, is preceded by another one, at $\hbar\omega \simeq 854.5$ Ry, attributable to the state $|1, 0, 0\rangle$, transitions to which are dipole-forbidden (due to a “transverse dipole” selection rule, see also Ventura et al. 1992). Similarly, dipole-forbidden transitions (i.e. opening of the $n = 1, s = 1$ continuum) are responsible for the jump of σ_{+} at 863.7 Ry.

The second, much weaker and narrower resonance (its autoionization width is only $\simeq 1.5 \times 10^{-4}$ Ry) in Fig. 3a is associated with the hydrogen-like quasi-bound state

$|1, 1, 2\rangle$. It is not observed in Fig. 3b because of the orders of magnitude stronger background absorption due to the transition to the continuum state $n_f = 1, s_f = -1$, which is allowed at $\theta \neq 0$ and whose threshold lies below this hydrogen-like quasi-bound level. In fact, there exist other Beutler–Fano resonances, related to the transitions to more excited quasi-bound states, but they are much too weak and narrow to play any role in the computed spectrum, so that we do not display them here. For the same reason, we also do not show the autoionizing resonances of σ_{\parallel} . For the longitudinal polarization, only transitions to the odd states are allowed at $\theta = 90^{\circ}$. Therefore only hydrogen-like autoionizing states can contribute to σ_{\parallel} . The corresponding resonances, however, are extremely weak and narrow ($\Gamma^a < 10^{-4}$ Ry).

Figure 4 shows the cross sections at a weaker field, $B = 10^{11}$ G. This field strength was not considered in Paper I because the adiabatic approximation may become too crude in this case. The present non-adiabatic treatment allows us to include this (and lower) field strength(s) into the consideration. Several Landau thresholds appear in the observationally relevant energy range in this case. Figure 5 demonstrates the resonances associated with these thresholds.

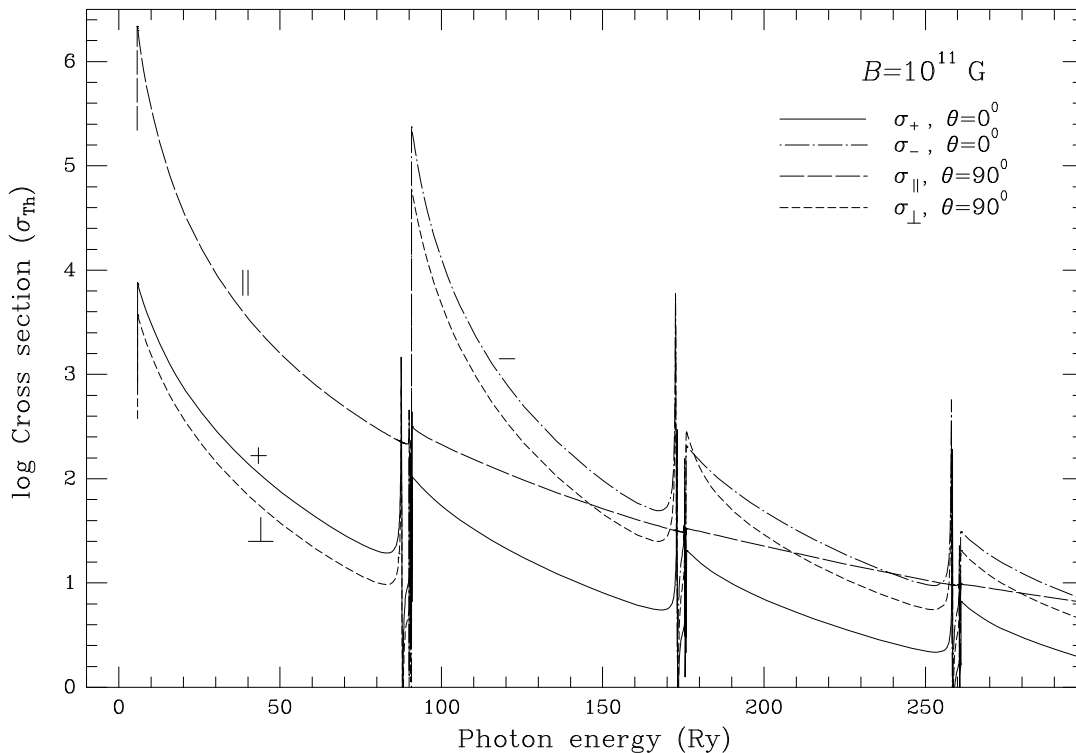


Fig. 4. Total cross sections of the photoionization of the ground state H atom at the magnetic field strength $B = 10^{11}$ G. Solid and dash-dot lines correspond to the right and left circular polarizations, respectively, at the incidence angle $\theta = 0^\circ$; short-dash and long-dash lines correspond to the transverse and longitudinal linear polarizations at $\theta = 90^\circ$

The cross section for the right circular polarization at $\theta = 0^\circ$ (solid lines in Figs. 4, 5) reveals a relatively broad resonance below each n -th Landau threshold associated with the tightly bound autoionizing states $|n, 1, 0\rangle$ (their peaks lie at $\hbar\omega = 87.6, 173.0$ and 258.4 Ry, and the autoionizing widths are $\Gamma^a = 0.014, 0.016$, and 0.014 Ry, for $n = 1, 2, 3$, respectively). A sequence of weaker and narrower resonances is further seen to converge to a corresponding threshold. These are related to the even hydrogen-like autoionizing states $|n, 1, 2\rangle, |n, 1, 4\rangle, \dots$

Analogous features for the left polarization (dot-dashed curves), associated with the states $|n, -1, 0\rangle, |n, -1, 2\rangle, \dots$, are seen for $n \geq 2$. The states $|1, -1, \nu\rangle$ are not coupled to the continuum (if the motion across the magnetic field is neglected) and do not contribute to the photoionization cross section. On the contrary, coupling of the states $|n, -1, 0\rangle$ for $n \geq 2$ is relatively strong (e. g., $\Gamma_{n-10}^a = 0.014$ and 0.016 Ry for $n = 2$ and 3 , respectively), and the corresponding resonances dominate in Fig. 5b,c. The cross section σ_\perp for the transverse polarization at $\theta = 90^\circ$ (short dashes) shows autoionization resonances associated with both $|n, 1, \nu\rangle$ (for $n \geq 1$) and $|n, -1, \nu\rangle$ (for $n \geq 2$) because $e_\perp = (e_+ + e_-)/\sqrt{2}$ is composed of both circular polarizations.

For the longitudinal polarization (long dashes), transitions to odd states are only allowed at $\theta = 90^\circ$. The

strongest resonance (at $\hbar\omega = 90.0$ Ry) in Fig. 5a corresponds to the state $|1, 0, 1\rangle$ ($\Gamma_{101}^a \simeq 0.0008$ Ry). Other odd-state resonances (barely seen in Fig. 5a) are considerably weaker. At higher Landau thresholds, all resonances of this type are weak and narrow.

The Beutler–Fano resonances in Figs. 3 and 5 were calculated assuming that autoionization is the only channel for decay of the quasi-bound states, so that other mechanisms which could lead to additional broadening of the resonances can be neglected. However, an excited state can always decay via spontaneous emission of a photon, and it is known (e. g., Wunner et al. 1983a) that the rate of the radiative decay can be very high in strong magnetic fields. The relative importance of the radiative and autoionization decays is determined by the relation between the autoionization width Γ^a and radiative width Γ^r . If $\Gamma^a \gg \Gamma^r$, then most electrons excited to the quasi-bound state rapidly escape into the continuum, and the shape of the photoabsorption resonances is determined by the autoionization. In the opposite case, spontaneous emission occurs faster than autoionization, so that absorption of radiation at resonance energies is not accompanied by photoionization, and the shape of the resonance is described by the Lorentz profile of the width Γ^r . Thus, it is important to compare Γ^a and Γ^r for a given level in order to evaluate which of the two processes is more important.

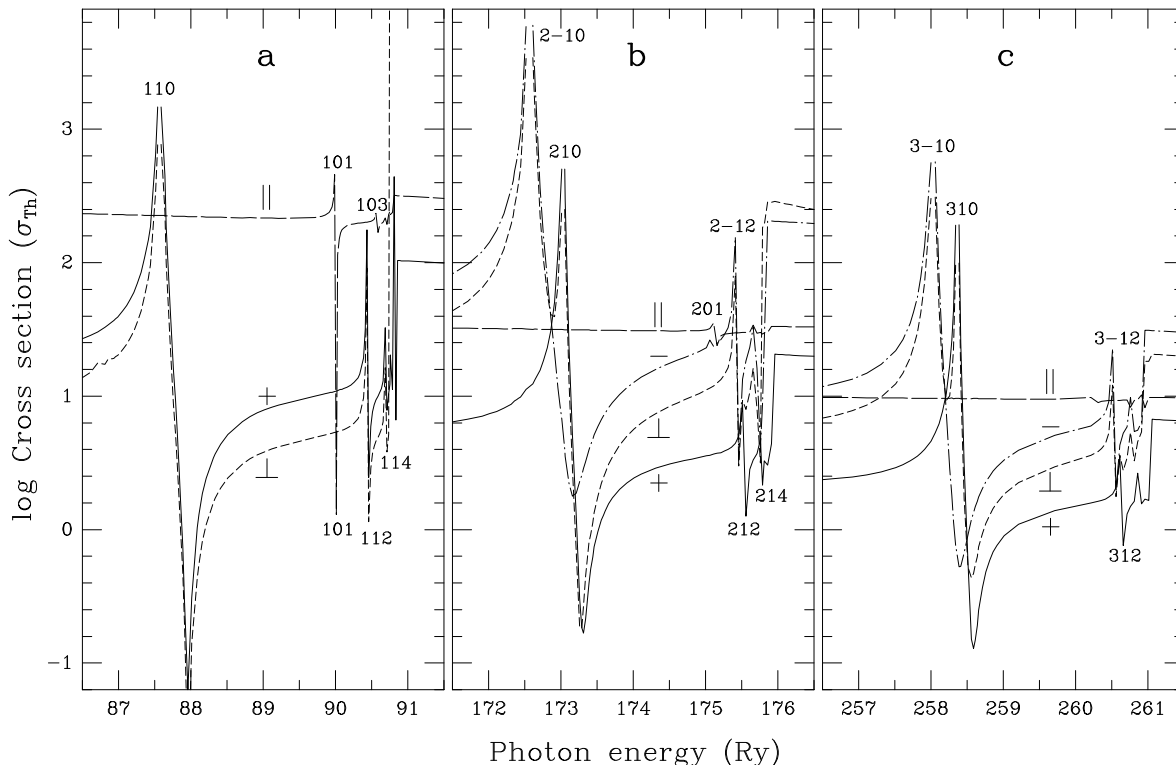


Fig. 5. Same as Fig. 4 for the energy ranges near the first three Landau thresholds (panels **a**, **b** and **c**, respectively)

The (total) autoionization widths for a few levels $|1, s, \nu\rangle$ and $|2, s, \nu\rangle$ are plotted as a function of B in Fig. 6. We see that they decrease with increasing B , being quite different for different autoionizing states. To understand qualitatively the behaviour of the widths, consider, for instance, the dependence of the coupling matrix element $U_{1s\nu,0}$, Eq. (15), which couples the $n = 1$ quasi-bound states to the $n = 0$ continuum, on the dimensionless magnetic field γ . A characteristic length, $\sim a_M = a_B \gamma^{-1/2}$, of the effective potential $V_{10}(z)$ in Eq. (15), which determines the limits of integration over z , is much smaller than a typical size, $\sim a_{\parallel}$ ($\sim a_B / \ln \gamma$ for $\nu = 0$, and $\sim a_B(\nu + 1)/2$ for $\nu > 0$), of the bound wave function $g_{1\nu}^{\text{ad}}(z)$. Therefore, in the integrand of Eq. (15), we have $g_{1\nu}^{\text{ad}}(z) \sim a_{\parallel}^{-1/2}$ for the even quasi-bound states, and $g_{1\nu}^{\text{ad}}(z) \sim a_{\parallel}^{-1/2}(a_M/a_{\parallel})$ for the odd states. The continuum wave function $g_0^{\text{ad}}(z)$ depends on the product $kz \sim (2\gamma)^{1/2}(z/a_B) \lesssim \sqrt{2}$. Taking into account that a characteristic magnitude of $V_{10}(z)$ is $\sim e^2/a_M \sim (e^2/a_B)\gamma^{1/2}$, we arrive at the following estimates for the autoionization widths at $\gamma \gg 1$: $\Gamma_{1s\nu}^{\text{a}} \propto \gamma^{-1/2} \ln \gamma$ for the tightly bound states, $\propto \gamma^{-1/2}$ for the hydrogen-like even states, and $\propto \gamma^{-3/2}$ for the hydrogen-like odd states. Similar behaviour is observed for the autoionization widths of the states with $n > 1$.

The radiative widths are mainly determined by the transitions $|ns\nu\rangle \rightarrow |n-1, s+1, \nu\rangle$; at $\gamma \gg 1$ the widths

depend only on the Landau quantum number n and the magnetic field,

$$\Gamma_n^{\text{r}} = \frac{8}{3} \alpha^3 n \gamma^2, \quad (39)$$

where α is the fine structure constant. In fact, (39) coincides with the well-known cyclotron width for cyclotron transitions of free electrons (e. g., Daugherty & Ventura 1978). We see from Fig. 6 that the radiative width exceeds all the autoionization widths at $B \gtrsim 6 \times 10^{11}$ G for $n = 1$, and $B \gtrsim 4 \times 10^{11}$ G for $n = 2$. This means that at very high magnetic fields the quasi-bound states are destroyed via radiative decay rather than via autoionization, and the shape of the resonances of the photoabsorption cross section is determined predominantly by the radiative broadening. At lower magnetic field, the shape of the resonances may be determined by different mechanisms for different quasi-bound levels. For instance, $\Gamma^{\text{a}} \gg \Gamma^{\text{r}}$ for the leading resonances in Fig. 5 (e.g. associated with the $|1, 1, 0\rangle$, $|2, -1, 0\rangle$, $|2, 1, 0\rangle$ states), whereas weaker resonances are subject to stronger radiative broadening.

To illustrate the expected effect of radiative deexcitation on the photoabsorption spectra, we added to Fig. 3 Lorentz profiles of the “bound-bound” transitions to the states $|1, 1, 0\rangle$ and $|1, -1, 0\rangle$ (dotted lines). The height and the shape of the profiles are determined by the radiative width ($\Gamma_1^{\text{r}} = 0.19$ Ry) and the oscillator strengths ($f_{000,110} = 3.1 \times 10^{-5}$, $f_{000,1-10} = 1.987$). Note

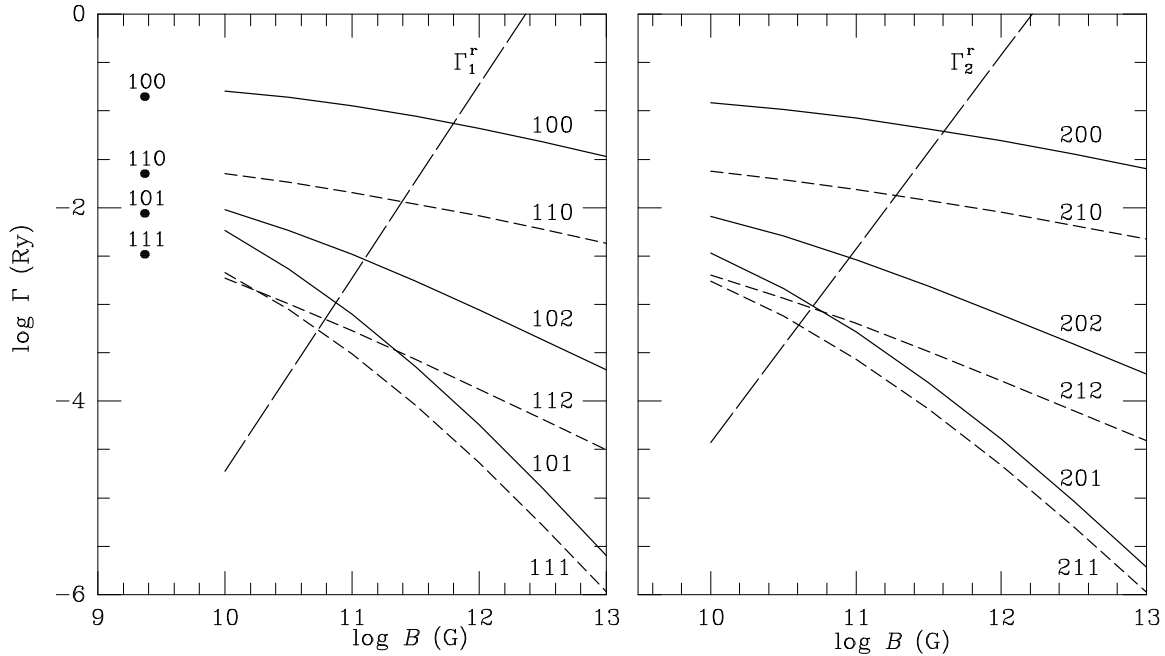


Fig. 6. Autoionization widths of a few states $|n, s, \nu\rangle$ (labels near the curves) vs. magnetic field. For $n = 2$, the total widths, $\Gamma_{2s\nu}^a = \Gamma_{2s\nu,0}^a + \Gamma_{2s\nu,1}^a$ are shown. The autoionization widths of the states $|2, -1, \nu\rangle$ coincide with those of the states $|1, 1, \nu\rangle$. The long-dashed curves show the radiative widths Γ_n^r of the levels with $n = 1$ and 2. The dots in the left panel show the values of the autoionization widths of the states (from top to bottom) $|1, 0, 0\rangle$, $|1, 1, 0\rangle$, $|1, 0, 1\rangle$ and $|1, 1, 1\rangle$ calculated by Friedrich and Chu (1983) for $B = 2.35 \times 10^9$ G ($\gamma = 1$)

that $|1, -1, 0\rangle$ is the truly bound state (for atoms at rest), and transitions to it are actually the strongest amongst all the transitions from the ground state, so that this “cyclotron absorption” dominates in the photoabsorption spectrum near the $n = 1$ Landau threshold. It should also be mentioned that the transition $|0, 0, 0\rangle \rightarrow |1, 1, 0\rangle$ is forbidden in the adiabatic approximation; its oscillator strength is provided by the admixture of $|1, 0, 0\rangle$ to the ground state, and $|0, 1, 0\rangle$ to the excited state.

5. Conclusions

We have studied photoionization cross sections of the hydrogen atom in magnetic fields $B \sim 10^{11} - 10^{13}$ G, typical for pulsars. We have used exact interaction matrix elements, including effects of finite proton mass, non-dipole and spin interaction terms. Unlike previous authors, we use *non-adiabatic* wave functions for the initial and final states of the atom. This accurate treatment yields the following conclusions.

First, it resolves the acute contradiction of previous works concerning the cross section for photons polarized transversely to the magnetic field at energies $\hbar\omega < \hbar\omega_c$. This cross section is finite, being orders of magnitude larger than σ_{Th} near the threshold, in agreement with Paper I. This is shown to have no connection with neglecting the spin interaction, as was assumed by KVH. Moreover, at $\omega \ll \omega_c$ the present results nearly coincide quantita-

tively with those in Paper I. We have proven that the zero values of σ_+ and σ_\perp , obtained by a number of authors following Schmitt et al. (1981), do not represent the reality but arise from their using the *velocity* representation of the interaction matrix elements in combination with the *adiabatic* approximation for the wave functions. This combination led those authors to miss the main contribution in the cross section.

Second, the non-adiabatic treatment includes autoionization of the quasi-discrete levels associated with the Landau excitations. These levels are considered as truly discrete in the adiabatic approximation. Autoionization manifests itself in the photoionization cross sections as Beutler–Fano resonances near the quasi-discrete levels; the shape of the resonances is determined by correlation between closed and open channels. We have calculated the autoionization widths for the most important resonances in a wide range of magnetic fields and have shown that they exceed the radiative widths if the magnetic field is not too strong, $B \lesssim 10^{11}$ G.

Third, we have shown that the adiabatic results significantly deviate from the exact ones not only near the resonances, but in a rather wide range of photon energies, unless the condition $\omega \ll \omega_c$ is satisfied. Above the Landau threshold, this deviation is due to correlation between different open photoionization channels.

In this paper we restrict ourselves to the particular case of an atom which does not move across the field. It

has been shown by Pavlov & Mészáros (1993), B&P and KVH that transverse atomic motion leads to the opening of additional channels of ionization. In the particular case of *slow* motion, however, our present consideration allows one to decide between the small transverse cross sections presented by KVH and orders of magnitude larger cross sections obtained by B&P — in favour of the larger ones.

Acknowledgements. This work was supported in part by INTAS (Grant 94-3834). A.Y.P. acknowledges partial support from RBRF (Grant 96-02-16870) and hospitality of the University of Crete and the Research Center of Crete (FORTH). The work of G.G.P. was supported by NASA Grant NAG5-2807. J.V. wishes to acknowledge partial support under NATO Grant Nr. CRG.931446.

Appendix A: derivation of Eqs. (30), (31)

In this section, we derive an approximate relation between non-adiabatic corrections which, according to Eq. (27), determine the interaction matrix element in the velocity representation for the transverse polarization, and the adiabatic overlap integral $\langle 0, f|0, i \rangle_{\parallel}$ which enters Eq. (29) for the matrix element in the length representation.

Let us consider the quantum states $|a\rangle$ and $|b\rangle$ ($n_a = n_b = 0$) belonging to adjacent s -manifolds: $s_a = s$, $s_b = s + 1$. The longitudinal coefficients in Eq. (2) are given by the set of coupled differential equations (3) with the effective potential (4). At $\gamma \gg 1$, the non-diagonal effective potentials are small compared to the diagonal ones, and the non-adiabatic admixtures $g_{n \neq 0}$ are small respectively. Retaining only the leading terms in the equation for $g_0(z)$, we have

$$\left[\frac{\hbar^2}{2\mu} \frac{d^2}{dz^2} + E_a - s \frac{m_e}{m_p} \hbar\omega_c \right] g_0^{(a)}(z) = V_{00}^{(s)}(z) g_0^{(a)}(z), \quad (\text{A1})$$

$$\begin{aligned} \left[\frac{\hbar^2}{2\mu} \frac{d^2}{dz^2} + E_b - (s+1) \frac{m_e}{m_p} \hbar\omega_c \right] g_0^{(b)}(z) \\ = V_{00}^{(s+1)}(z) g_0^{(b)}(z). \end{aligned} \quad (\text{A2})$$

Keeping the first-order terms in the equation for $g_1^{(a)}(z)$, we obtain

$$\begin{aligned} \left[\frac{\hbar^2}{2\mu} \frac{d^2}{dz^2} + E_a - \left(1 + s \frac{m_e}{m_p}\right) \hbar\omega_c \right] g_1^{(a)}(z) \\ = V_{11}^{(s)}(z) g_1^{(a)}(z) + V_{01}^{(s)}(z) g_0^{(a)}(z). \end{aligned} \quad (\text{A3})$$

Here the terms $V_{n1}g_n$ with $n \geq 2$ are neglected.

Multiplying Eq. (A1) by $g_0^{(b)}(z)$ and Eq. (A2) by $g_0^{(a)}(z)$, subtracting them by terms and integrating over z , we arrive at the approximate relation

$$\begin{aligned} \left(E_a - E_b + \frac{m_e}{m_p} \hbar\omega_c \right) \langle 0, a|0, b \rangle_{\parallel} \\ = \langle 0, a|V_{00}^{(s)} - V_{00}^{(s+1)}|0, b \rangle_{\parallel}. \end{aligned} \quad (\text{A4})$$

Analogously, from Eqs. (A2) and (A3) we obtain

$$\begin{aligned} \left[E_a - E_b - \left(1 - \frac{m_e}{m_p}\right) \hbar\omega_c \right] \langle 1, a|0, b \rangle_{\parallel} \\ = \langle 0, a|V_{01}^{(s)}|0, b \rangle_{\parallel} + \langle 1, a|V_{11}^{(s)} - V_{00}^{(s+1)}|0, b \rangle_{\parallel}. \end{aligned} \quad (\text{A5})$$

The second term on the right-hand side should be omitted in the approximation considered. Indeed, according to Eq. (4), the difference of two diagonal effective potentials can be expressed in terms of non-diagonal ones,

$$\begin{aligned} V_{11}^{(s)}(z) - V_{00}^{(s+1)}(z) = (s+1)^{-1/2} \\ \times \left[\sqrt{s+2} V_{02}^{(s)}(z) - V_{01}^{(s)}(z) \right], \end{aligned} \quad (\text{A6})$$

and thus the last term in Eq. (A5) represents a second order correction. Analogously, the difference on the right-hand side of Eq. (A4) equals

$$V_{00}^{(s)}(z) - V_{00}^{(s+1)}(z) = (s+1)^{-1/2} V_{01}^{(s)}(z). \quad (\text{A7})$$

Comparison of Eqs. (A4) and (A5) yields now:

$$\frac{\langle 1, a|0, b \rangle_{\parallel}}{\langle 0, a|0, b \rangle_{\parallel}} \approx \sqrt{s+1} \frac{E_a - E_b + (m_e/m_p)\hbar\omega_c}{E_a - E_b - (1 - m_e/m_p)\hbar\omega_c}. \quad (\text{A8})$$

Applying this result to radiative transitions between a lower state $|i\rangle$ and an upper state $|f\rangle$, neglecting m_e/m_p in the denominator, and assuming $\omega \ll \omega_c$, we arrive at Eqs. (30) and (31).

Appendix B: details of computation

B.1. Solving the Schrödinger equation

Bound state wave functions are calculated using the multiconfigurational Hartree–Fock technique described in Paper II.

Continuum wave functions are sought in the form (2), separately for each z -parity. The set of Eqs. (3) for the longitudinal coefficients is rearranged in two coupled subsystems, which are solved by two-step iterations. In the first step, the equations for the open channels ($n, n' = n_{\min}, \dots, n_0 - 1$) are solved, the contribution to the right-hand side from the other group of orbitals ($n' = n_0, \dots, n_{\max}$) being fixed. In the second step, the longitudinal wave functions of the closed channels ($n, n' \geq n_0$) are adjusted to the open-channel functions ($n' < n_0$) found in the preceding step. The procedure is then repeated; typically, a few such iterations are sufficient to reach convergence. The only exception occurs in the resonance energy region, where the number of iterations increases up to 20–30, and the method finally fails in narrow energy regions corresponding to the very top of the peaks. Nevertheless, as can be seen in our figures, we are still able to trace substantial parts of the resonance profiles.

The first step of each iteration is performed by the outward integration, employing the explicit fourth-order

Runge–Kutta scheme (e.g., Fletcher 1988) for the vector function $\mathbf{g} = (g_0^{(f)}, \dots, g_{n_0-1}^{(f)})$. The integration extends to the point $z_0 \sim 10^2 a_m$, where the off-diagonal effective potentials become negligible. The second step, solving the longitudinal equations for $g_{n \geq n_0}$ provided that $g_{n < n_0}$ are fixed, does not differ from that described in Paper II. After the iterative process ends, one extra integration for each orbital is required to proceed beyond z_0 , where the orbitals are already uncoupled.

B.2. Rearrangement

The outward integration for the open channels is performed with the initial conditions arbitrarily chosen as $g_n(0) = g'_n(0) = 0$ for all $n < n_0$ except $n = j$, whereas we chose $g_j(0) = 1$ or $g'_j(0) = 1$ depending on parity. In this way we obtain an arbitrary set of n_0 linearly independent wave functions $\psi^{(j, \text{arb})}(\mathbf{r})$, $j = n_{\min}, \dots, n_0 - 1$. This set has to be rearranged, in order to meet the asymptotic conditions (6):

$$g_{n'}^{(n, \text{real})}(z) = \sum_{j=n_{\min}}^{n_0-1} a_{nj} g_n^{(j, \text{arb})}(z), \quad (\text{B1})$$

where the coefficients a_{nj} constitute the rearrangement matrix A . In order to obtain A , first, the integration is extended to a point $z_{\text{as}} \gg e^2 / \min(E_f - E_{n_s f}^\perp)$, where the asymptotic behaviour is reached. The minimum longitudinal energy here is to be taken over all open channels, i.e. for $n = 0, \dots, n_0 - 1$. An outermost part of this integration may be performed by a faster scheme, cf. Paper I. Then, using Eq. (B1) together with Eq. (6), we arrive at the algebraic system:

$$\begin{aligned} \sum_{j=n_{\min}}^{n_0-1} g_n^{(j, \text{arb})}(z_{\text{as}}) a_{nj} - \cos \phi_{n'}(z_{\text{as}}) R_{nn'} \\ = \delta_{nn'} \sin \phi_n(z_{\text{as}}), \\ \sum_{j=n_{\min}}^{n_0-1} \frac{d}{dz} g_n^{(j, \text{arb})}(z_{\text{as}}) a_{nj} + \phi'_{n'}(z_{\text{as}}) \sin \phi_{n'}(z_{\text{as}}) R_{nn'} \\ = \delta_{nn'} \phi'_n(z_{\text{as}}) \cos \phi_n(z_{\text{as}}), \quad n, n' = 0, \dots, n_0 - 1, \quad (\text{B2}) \end{aligned}$$

the phase ϕ_n being defined in Eq. (7). For each given n , the $2(n_0 - n_{\min}) \times 2(n_0 - n_{\min})$ system (B2) is solved to get the n th row of the matrices A and R . Since the matrix of this algebraic system does not depend on n , the FACT/SOLVE code (Fletcher 1988) is most useful.

Longitudinal matrix elements, which enter Eq. (21), are calculated along with the functions $g^{(j, \text{arb})}$ at the last stage of the integration for each specific j . They still need to be transformed into the matrix elements for the outgoing states. According to Eqs. (B1) and (10), this transformation of the array of matrix elements is performed by the matrix $i\sqrt{2/L_z}(1 + iR)^{-1}A$, which acts on the subscript j related to a channel. The square root multiplier ensures the necessary normalization (Sect. 2.2).

References

- Bezchastnov, V.G., Potekhin, A.Y. 1994, *J. Phys. B*, 27, 3349 (B&P)
- Canuto, V., Ventura, J. 1977, *Fundam. Cosmic Phys.*, 2, 203
- Daugherty, J.K., Ventura, J. 1978, *Phys. Rev. D*, 18, 1053
- Delande, D., Bommier, A., Gay, J.C. 1991, *Phys. Rev. Lett.*, 66, 141
- Fletcher, C.A.J. 1988, *Computational Techniques for Fluid Dynamics*, Pt. I, Springer, Berlin
- Friedrich, H. 1991, *Theoretical Atomic Physics*, Springer-Verlag, Berlin
- Friedrich, H., Chu, M. 1983, *Phys. Rev. A*, 28, 1423
- Gnedin, Yu.N., Pavlov, G.G., Tsygan, A.I. 1974, *Sov. Phys.-JETP*, 39, 301
- Hasegawa, H., Howard, R.E. 1961, *J. Phys. Chem. Solids*, 21, 179
- Herold, H., Ruder, H., Wunner, G. 1981, *J. Phys. B*, 14, 751
- Kopidakis, N., Ventura, J., Herold, H. 1996, *A&A*, 308, 747 (KVVH)
- Mega, C., Herold, H., Rösner, W., Ruder, H., Wunner, G. 1984, *Phys. Rev. A*, 30, 1507
- Merani, N., Main, J., Wunner, G. 1995, *A&A*, 298, 193
- Miller, M.C., Neuhauser, D. 1991, *MNRAS*, 253, 107
- Ögelman, H. 1995, X-ray observations of cooling neutron stars, in M.A. Alpar, Ü. Kiziloğlu, J. van Paradijs (eds.), *The Lives of the Neutron Stars* (NATO ASI Ser. C, v. 450), Kluwer, Dordrecht, p. 101
- O'Mahony, P.F., Mota-Furtado, F. 1991, *Phys. Rev. Lett.*, 67, 2283
- Pavlov, G.G., Mészáros, P. 1993, *ApJ*, 416, 752
- Pavlov G.G., Shibano Y.A., Zavlin V.E., Meyer R.D. 1995, Neutron star atmospheres, in M.A. Alpar, Ü. Kiziloğlu, J. van Paradijs (eds.), *The Lives of the Neutron Stars* (NATO ASI Ser. C, v. 450), Kluwer, Dordrecht, p. 71
- Potekhin, A.Y. 1994, *J. Phys. B*, 27, 1073 (Paper II)
- Potekhin, A.Y., Pavlov, G.G. 1993, *ApJ*, 407, 330 (Paper I)
- Rösner, W., Wunner, G., Herold, H., Ruder, H. 1984, *J. Phys. B*, 17, 29
- Schmitt, W., Herold, H., Ruder, H., Wunner, G. 1981, *A&A*, 94, 194
- Seaton, M.J. 1983, *Rep. Progr. Phys.*, 46, 167
- Simola, J., Virtamo, J. 1978, *J. Phys. B*, 11, 3309
- Sokolov, A.A., Ternov, I.M. 1968, *Synchrotron Radiation*, Akademie-Verlag, Berlin
- Ventura, J., Herold, H., Ruder, H., Geyer, F. 1992, *A&A*, 261, 235
- Wunner, G., Herold, H., Ruder, H., 1983a, *J. Phys. B*, 16, 2937
- Wunner, G., Ruder, H., Herold, H., Schmitt, W. 1983b, *A&A*, 117, 156
- Xi, J., Wu, L., He, X., Li, B. 1992, *Phys. Rev. A*, 46, 5806